J Solid State Electrochem (2006) 10: 967–979
DOI 10.1007/s10008-005-0033-7

ORIGINAL PAPER

V. Dharuman · K. Chandrasekara Pillai

RuO_2 electrode surface effects in electrocatalytic oxidation of glucose

Received: 25 May 2005 / Revised: 1 June 2005 / Accepted: 9 June 2005 / Published online: 10 August 2005

Abstract We have studied the electrocatalytic activity of RuO_2-PVC film electrodes, fabricated using RuO_2 powders prepared at five different temperatures, viz., 300, 400, 500, 600 and 700°C, for the oxidation of glucose in high alkaline media, 1 to 3 M NaOH. The RuO_2-PVC film electrodes have been first characterized in 1 to 3 M NaOH solution by cyclic voltammetry (CV) and rotating disc electrode (RDE) techniques in a wide potential range −1,100 to 450 mV (SCE), and three redox pairs representing Ru(IV)/Ru(III), Ru(VI)/Ru(IV) and Ru(VII)/Ru(VI) transitions have been identified. The voltammetric peaks at low sweep rates have been analyzed using surface activity theory formulated for interacting electroactive adsorption sites, and interaction terms have been evaluated. The total voltammetric surface charges have been analyzed as per Trassatti's formalism with respect to their dependence on potential sweep rate, and charges associated with less accessible and more accessible surface sites have been calculated. For glucose oxidation, the results have indicated that RuO_2 (700°C)-PVC electrode shows two oxidation peaks in contrast to RuO_2 (300°C)-PVC electrode. Also, RuO_2 (700°C)-PVC electrode exhibits higher intrinsic electrocatalytic activity than the 300°C electrode, although the former possesses lower electrochemically active surface area. Additionally, kinetic analyses made from RDE results with reference to Michealis–Menten (MM) enzyme catalysis has shown that RuO_2 (700°C) electrode possesses extended glucose-sensing range in terms of MM kinetic constant, K_M, compared to other electrodes. Possible reasons for such differences in the behavior of the electrodes of different temperatures towards glucose oxidation are identified from studies on oxidation of glucose in solutions of different pH, oxidation of different glucose derivatives, and also from physicochemical results from BET, XRD, SEM, DTGA, XPS analysis of RuO_2 powder samples.

Keywords RuO_2-PVC film electrode · Oxide preparation temperature · Glucose oxidation · Electrocatalytic activity · Michaelis–Menten kinetics

V. Dharuman · K. Chandrasekara Pillai (✉)
Department of Physical Chemistry, University of Madras, Guindy Campus, Chennai, 600 025, India
E-mail: kc_pillai@yahoo.com
Fax: +91-44-2235-2494

V. Dharuman
Department of Biotechnical Microsystems, Fraunhofer Institute for Silicon Technology, Fraunhofer strasse 1, 25524, Itzehoe, Germany

Introduction

The literature on the electrooxidation of carbohydrates, especially, glucose, shows that it can be oxidized directly on various metal electrodes, such as, Pt [1–3], Cu [4, 5], Au [6, 7], Ag [8], Ni [9, 10], Co [11] and on cobalt phthalocyanine-modified electrode [12]. In recent times a few conducting metal oxides like tungsten oxide [13], ruthenium oxide [14–17], and iridium oxide [18] have been studied for glucose oxidation revealing many useful and unique properties, like, reduced operation over potential and enhanced efficiency of the glucose oxidation reaction. In particular ruthenium dioxide has received special attention due to its high metallic conductivity, unusual stability, presence of Ru in several oxidation states (Ru(III), Ru(IV), Ru(VI), Ru(VII)) within the potential region in which solvent (water) is stable, and excellent activity towards electrocatalytic oxidation of carbohydrates and several other organic compounds [19–30].

Activity of pure metal electrodes on glucose [1–10] reveals the following aspects: glucose oxidation is a potential-dependent and multi-step multi-electron transfer reaction; the rate of oxidation reaction and the type of reaction intermediates formed depend on the nature and structure of the electrode material. For example, glucose was found to react differently on different single crystals of Pt [2] and Au [7], and in this respect still research is being conducted with many advanced in-situ spectroscopic techniques to identify the reaction intermediates to obtain intricate details of the

oxidation mechanism. We expect a similar electrode structure-sensitive glucose oxidation reaction with RuO_2 electrode as well. With RuO_2-based electrode material it is significantly convenient to impart structural and morphological changes by varying the electrode preparation temperature [31–33].

Ruthenium-dioxide-coated electrodes were widely investigated, and RuO_2 electrodes are more traditionally prepared from its chloride salt by high temperature pyrolysis technique, wherein the oxide is directly formed on suitable substrates like Ti, Ta, Pt or silica glass, Ti being the most predominantly used [31, 32]. Literature reports [31] indicate that RuO_2 formation starts from 285°C, with complete formation at 450°C, and continuing up to 850°C. But note that in preparing RuO_2 coatings by direct thermal decomposition at temperatures higher than 500°C, problems arise at the contact between the support and the active layer, such as, interphase swelling, formation of fragile overlayers, interdiffusion etc. [31, 32]. Recently, we overcame this problem by initially preparing the RuO_2 powders at high temperatures even up to 700°C, and then coating a Pt electrode surface with a mixture of RuO_2 powders and PVC (80:20 w/w%) in THF solvent. This method appears to be more convenient, leading to a well-bonded and mechanically stable layer on Pt surface. RuO_2-PVC film electrodes were prepared previously by the above method in the temperature range 300 to 700°C and characterized in solutions of various pH, 1 to 14 [33].

In this paper, we report electrocatalytic oxidation of glucose in NaOH solutions of 1 to 3 M concentration at RuO_2-PVC film electrodes, fabricated using oxides prepared at five different temperatures viz., 300, 400, 500, 600 and 700°C, and illustrate that the reaction mechanism and the extent of oxidation of glucose, indeed, strongly depend on the morphological and structural features of these electrodes. Interestingly, higher intrinsic electrocatalytic activity and extended linearity for glucose sensing are observed for RuO_2 (700°C)-PVC electrode and not for RuO_2 (300°C)-PVC electrode, although the 700°C electrode possesses smaller surface charge and lower electrochemically active surface area. The possible reasons are exploited with supporting results from other non-electrochemical techniques like BET, X-ray diffractometry (XRD), scanning electron microscopy (SEM), differential thermogravimetry (DTGA), and X-ray photoelectron spectroscopy (XPS). In the first part of the work RuO_2-PVC film electrodes are characterized in 1 to 3 M high alkaline solutions, followed by electrooxidation of glucose using both CV and RDE techniques.

Experimental details

Chemicals

Glucose, NaOH and tetrahydrofuran (THF) of HPLC grade were obtained from Sd fine chemicals, India. $RuCl_3.xH_2O$ was from Arora Matthey, India, and poly(vinylchloride) (PVC) was from Fluka. All the experimental solutions were prepared using doubly distilled water.

Experimental

Cyclic voltammograms were recorded using Wenking potentiostat (ST 72) coupled with a Wenking signal generator (VSG 83) and a Graptech X-Y-t recorder (WX 2300). RDE experiments were carried out using Analytical rotator, Pine Instruments USA. A home-made three-compartment glassy cell consisting of a main body (200 ml) and a smaller compartment, isolated from the main body by coarse glass frit containing a large surface area (4 cm^2) Pt foil employed as auxiliary electrode, was used. The working electrode was placed in the center of the main body which also contained the reference electrode (SCE) mounted in a Luggin capillary to minimize the iR drop.

RuO_2-PVC film electrode preparation

RuO_2-PVC film electrodes were prepared as described elsewhere [33]. Briefly, $RuCl_3.xH_2O$ was heated in a muffle furnace at preset preparation temperature in presence of a stream of O_2 for 12 h with intermittent cooling and grinding. Finally the oxide samples were water-washed thoroughly for the removal of trace quantities of Cl^-, dried in air oven at 110°C for 12 h and stored in desiccator. RuO_2 powder was mixed with PVC in 4:1 (wt%) ratio in dry THF, and the paste like slurry was coated on to a pretreated Pt electrode of 5 mm diameter. It was then dried at room temperature for 2 days. The effective loading was around 40 mg cm^{-2}. Prior to coating, Pt was pretreated by polishing it with an emery paper (No. 800, Carborandum Universal, India) followed by washing in 20% HCl and water.

Results and discussion

Characterization of electrodes

The electrochemical characterization of conductive metallic oxide electrodes is generally accomplished through cyclic voltammetry. This technique is very powerful for in situ characterization of electrode surfaces, its quantitative and qualitative behavior being intimately related to the surface conditions of the electrode. RuO_2-PVC film electrodes, fabricated using oxides prepared at different temperatures ca. 300 to 700° C, have already been characterized in solutions of different pH, 0 to 14 [33]. The following is the detailed analysis in different NaOH solutions. Initially, RuO_2 (700°C)-PVC film electrode is studied in detail in 3 M NaOH followed by other NaOH solutions. Subsequent to this, other temperature RuO_2 electrodes are investigated.

Cyclic voltammetric behavior of RuO_2 (700°C)-PVC film electrode in NaOH solutions of different concentrations

Figure 1 illustrates the cyclic voltammograms, CV, recorded for RuO_2 (700°C)-PVC film electrode in 3 M NaOH at different scan rates (v) in the potential range −1,100 to 450 mV. The voltammetric curve within the potential window for oxygen and hydrogen evolution reactions shows three pairs of reversible peaks localized at −400 to −350 mV, −100 to 100 mV, and 300 to 400 mV, corresponding, respectively, to Ru(IV)/Ru(III), Ru(VI)/Ru(IV), and Ru(VII)/Ru(VI) solid-state redox transitions, in broad agreement with the one described previously in NaOH solution of similar concentration for Ti/RuO_2 electrode prepared by direct thermal decomposition of $RuCl_3$ on Ti at 425°C [34]. The peaks are designated as A1/C1, A2/C2, and A3/C3 for further discussion.

The peak currents of anodic and cathodic peaks increased with scan rate. The couple A1/C1 is less well-defined than the other two. A linear relation is observed for log(peak current density) with log(scan rate); however, with two slopes ca. 1 in the lower scan rate region (10–150 mV s^{-1} for A3/C3 and 20–300 mV s^{-1} for A2/C2), and 0.5 at higher scan rates (150–800 mV s^{-1} for A3/C3 and 300–800 mV s^{-1} for A2/C2). The peak potential, E_p, is invariant with scan rate at slower scan rates, but is displaced anodically at high scan rates, by 40 and 50 mV per decade increase in sweep rate for A3 and A2 peaks, respectively. All these results support the surface redox-state behavior of the system at low scan rates, and diffusional behavior at high scan rates; the rate determining diffusional process in the latter case occurring either in solution bulk or in RuO_2 material. The RDE technique is suitable to delineate the solution mass transfer from a similar process in electrode solid material [35]. The peak position and peak currents for all the three pairs of peaks are not dependent on electrode rotation, signifying that the surface electron transfer processes of the three pairs of peaks is coupled to the diffusion of electrolyte ion occurring within the solid matrix [35].

In aqueous solution of NaOH of varying concentrations ca. 2, 1.5, and 1 M, the back ground current and the peak currents decreased systematically and the $E_{1/2}$, obtained as $(E_{pa} + E_{pc})/2$, is shifted anodically with decrease in NaOH concentration. This is true for all the three redox couples. The shift of $E_{1/2}$ with $\log(c_{OH})$ is shown in Fig. 2. The coefficient $[\partial E_{1/2}/\partial \log(c_{OH})]$ is −85, −82 and −95 mV decade^{-1} for A1/C1, A2/C2 and A3/C3, respectively. These values are close to −3/2 (2.303RT/F) observed by Lyons and Burke for 450°C pyrolyzed Ti/RuO_2 electrode in NaOH solutions of concentrations 1 to 6 M [34]. Thus, the solid-state redox reactions of RuO_2(700°C)-PVC film electrode in 1 to 3 M NaOH solutions can be described as follows:

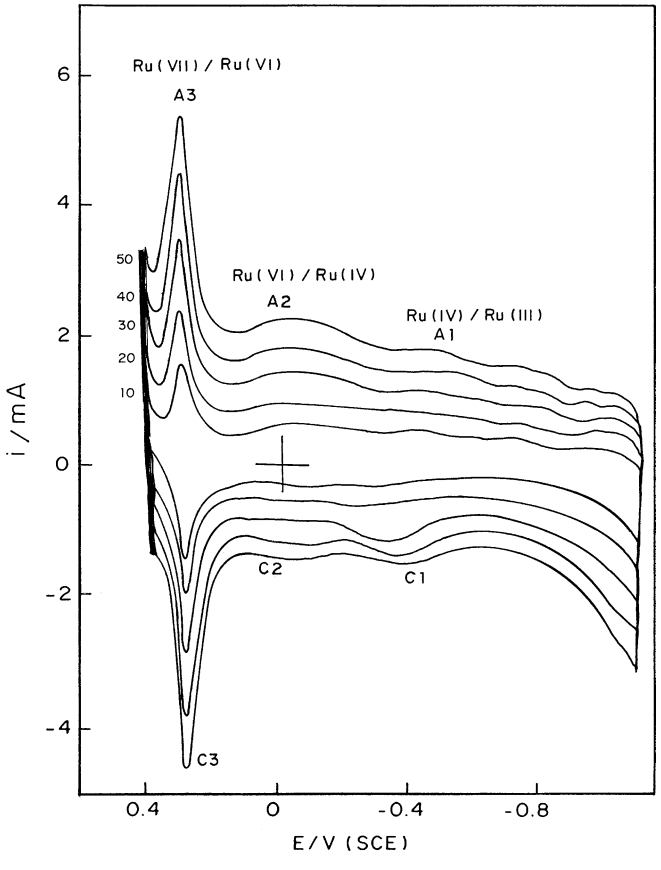

Fig. 1 Cyclic voltammograms of RuO_2 (700°C)-PVC film electrode in 3 M NaOH at various sweep rates (mV s^{-1}) indicated in the figure. Electrode geometric area = 0.0707 cm^2

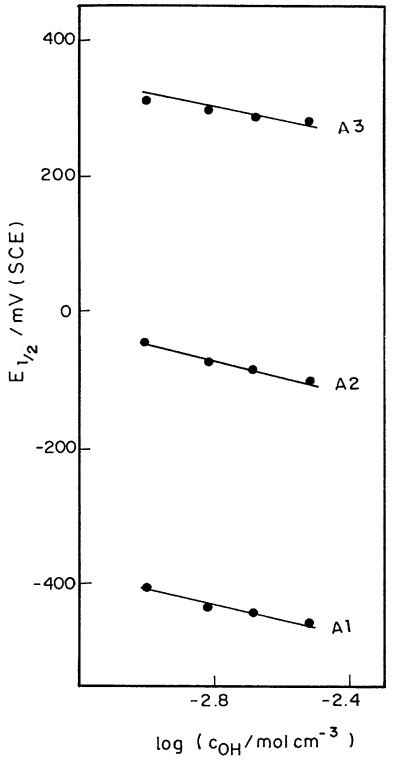

Fig. 2 $E_{1/2}$ versus $\log(c_{OH})$ plots for A1/C1, A2/C2, and A3/C3 redox couples of RuO_2 (700°C)-PVC film electrode

A1/C1

$$(--O--)_2Ru^{III}O^-(H_2O)_3 + 1.25OH^- \rightleftarrows (--O--)_2Ru^{IV}O^-[(OH)_{1.25}]^{-0.25}(H_2O)_{1.75} + 1.25H_2O + e \quad (1)$$

A2/C2

$$(--O--)_2Ru^{IV}O^-[(OH)_{1.25}]^{-0.25}(H_2O)_{1.75} + 2.5OH^- \rightleftarrows (--O--)_2Ru^{VI}[O_{1.75}]^{-1.75}(OH)_{2.25} + 2.5H_2O + 2e \quad (2)$$

A3/C3:

$$(--O--)_2Ru^{VI}[O_{1.75}]^{-1.75}(OH)_{2.25} + 1.25OH^- \rightleftarrows (--O--)_2Ru^{VII}[O_3]^{-2}(OH) + 1.25H_2O + e \quad (3)$$

Considering the voltammetric behavior at low sweep rates, the results, although, indicate reversible surface reactions (symmetrical peak shapes, nearly equal anodic and cathodic peak heights, linear increase of i_{pa} versus v, scan-rate-independent E_{pa}, and electrode-rotation-independent CV traces) for all the three redox pairs, nevertheless peak-to-peak separation ($E_{pa} - E_{pc}$) and the potential of full width at half maximum (E_{FWHM}) are not equal to those predicted for ideal systems [36–38], namely, zero and (90/n) mV (where n is the number of electrons transferred per electroactive site), respectively. The deviation from ideal behavior may arise due to the site-to-site interactions (thermodynamic effect), slow charge transfer (kinetic effect), or large uncompensated electrolyte resistance effects [37–39]. Following this, the interaction term r of each of the redox pairs ca. A2/C2 and A3/C3, associated with the RuO_2 (700°C)-PVC film electrode is estimated from the relationship

$$i_{pa} = \frac{nFq_s v}{RT(4 - 2r\Gamma_s)} \quad (4)$$

formulated for interacting electroactive adsorption sites [37–39]. Here q_s (in coulombs) is the charge due to solid-state redox transition and Γ_s (in mol cm^{-2}) is the surface concentration of the redox sites, related to each other, as

$$q_s = nFA_{geo}\Gamma_s \quad (5)$$

A_{geo} (in cm^2) is the geometric area of the electrode, and R, T and F have their usual significance. The ratio of i_{pa}–v slope to the charge q_s gives, from Eq. 4, $nF/[RT(4-2r\Gamma_s)]$, from which r is evaluated. q_s for these calculations was obtained integrating the i–E curve over the potential interval between the foot of the oxidation process and the peak ending for low v, typically 5 mV s^{-1}.

For A3 (Ru(VII)/Ru(VI) transition), with $n=1$ and $\Gamma_{s3} = 3.69\times10^{-7}$ mol cm^{-2} (estimated from the charge q_{s3} under A3 peak), r_{A3} is calculated to be -2.16×10^6 cm^2 mol^{-1}. For A2 (Ru(VI)/Ru(IV) transition), $r_{A2} = -4.40\times10^7$ cm^2 mol^{-1} with $n=2$ and $\Gamma_{s2} = 1.53\times10^{-7}$ mol cm^{-2}. The negative r for A2 and A3 indicates that repulsive interaction exists amongst the redox sites of A3/C3 and A2/C2 in the surface layer. The greater negative value for A2/C2, by one order, indicates that repulsion is more for A2/C2 than the A3/C3 case. The observation that peak A2 is quite broad and charge possessed by this peak (1.05 mC) is less than double the charge of peak A3 (2×2.5 mC), in spite of the fact that A2 involves two electrons while A3 involves only one electron, is probably due to the greater negative interaction associated with A2.

Note that the r values -2.16×10^6 cm^2 mol^{-1} and -4.40×10^7 cm^2 mol^{-1} for A3 and A2 in 3 M NaOH can be compared with their respective values ca. 7.24×10^6 cm^2 mol^{-1} and -1.26×10^7 cm^2 mol^{-1} in 1 M NaOH [33]. It can be noticed that with increase in NaOH concentration from 1 to 3 M, the interaction in the adsorption layer becomes increasingly repulsive for both A3 and A2. This behavior can be associated with oxide solvation. In aqueous medium the oxide surface is covered by OH^- groups forming hydroxylated species [34, 40] which are responsible for solid-state redox transitions (Eqs. 1, 2, 3) and associated surface charge. An increase in surface hydroxylation with an increase in NaOH concentration, consequently, promoting repulsion in the surface layer, is reasonable. This is confirmed by total voltammetric surface charge for different NaOH solutions. Figure 3 shows anodic and cathodic charge densities, q_a and q_c respectively, calculated based on the electrode geometric area as a function of NaOH concentration for 700°C electrode (and also for other electrodes, see later). q_a and q_c were obtained integrating the i–E curve of the respective NaOH solution over the complete potential interval −1,100 to 450 mV for $v = 5$ mV s^{-1}. Figure 3 shows that for 700°C electrode, there is a slight, but definite, increase with NaOH concentration, in q_a and q_c.

Note that the potential region −1,100 to 450 mV comprises solid-state redox reactions involving the various oxidation states of Ru (Eqs. 1, 2, 3) superimposed on the double-layer-charging [31, 32]. It appears, therefore, reasonable to consider that q_a and q_c are composed of greater contribution by the redox transitions and only marginally by double-layer-charging [27, 28]. Thus, the charge values can be taken as a relative measure of active surface sites and can be used to follow the electrochemically active surface area of the electrodes [27, 28, 41].

RuO_2-PVC film electrodes of different temperatures in NaOH solutions of different concentrations

Typical CV curves measured in 3 M NaOH for RuO_2 electrodes of five different temperatures 700, 600, 500, 400 and 300°C in the potential region −1,100 to 450 mV are shown in Fig. 4. It can be seen that when oxide preparation temperature is decreased from 700 to 300°C, the overall voltammetric current increases gradually and

the surface redox peaks also show an increase in intensity. However, the peaks loose their sharpness and become broader for low temperature samples. The electrochemistry of different temperature electrodes can be now conveniently understood using total voltammetric surface charge, as a criterion, and analyzing the potential sweep rate dependence of q_a and q_c, as per Trasatti formalism [41].

For this purpose, CV curves over the entire potential range −1,100 to 450 mV were integrated at various scan rates for all the five temperature electrodes and for all the four NaOH solutions. Typical plots of q_a and q_c for the five electrodes in 3 M NaOH are given in Fig. 5 as a function of scan rate. Note that at any particular scan rate, there is a systematic increase in q_a and q_c with decrease in oxide preparation temperature from 700 to 300°C. This can be understood as: with decrease in oxide preparation temperature, high surface area material results with the existence of countless fissures, cracks etc. [31, 32]. Due to this characteristic morphology of thermal oxides normally two regions can be distinguished: (1) the external oxide/solution interface and (2) the internal oxide/solution interface located inside the fissures and cracks. It is the less accessibility of these more internal, difficult-to-reach surface sites in the pores and cracks for the diffusing OH^- ion for the electron transfer reactions (Eqs. 1, 2, 3) that is responsible for the steady decrease of q_a (q_c) with potential sweep rate, as observed in Fig. 5, for different temperature electrodes. Interestingly, for high temperature sample ca. 700°C, q remains nearly independent of sweep rate signifying that the "screened" surface is relatively smaller for this electrode.

The charges associated with external oxide/solution interface (q^*_{out}) and internal oxide/solution interface (q^*_{in}) are calculated from experimental q_a values. According to Ardizzone et al. [41], for an oxide material, the measured voltammetric charge, q_a, at various scan rates can be linearized if $1/q_a$ is plotted against $v^{1/2}$. The linear extrapolation to $v \to 0$ gives q^*_{tot}, the surface charge arising due to infinitely slow OH^- ion exchange, and thus denoting the charge related to whole active surface. That is

$$\frac{1}{q_a} = \frac{1}{q^*_{tot}} + \text{constant1}\ (v^{1/2}) \qquad (6)$$

On the other hand, a plot of q_a against $v^{-1/2}$, and extrapolation to $v \to \infty$ gives an intercept of q^*_{out}, the amount of charge related to outer surface of the oxide

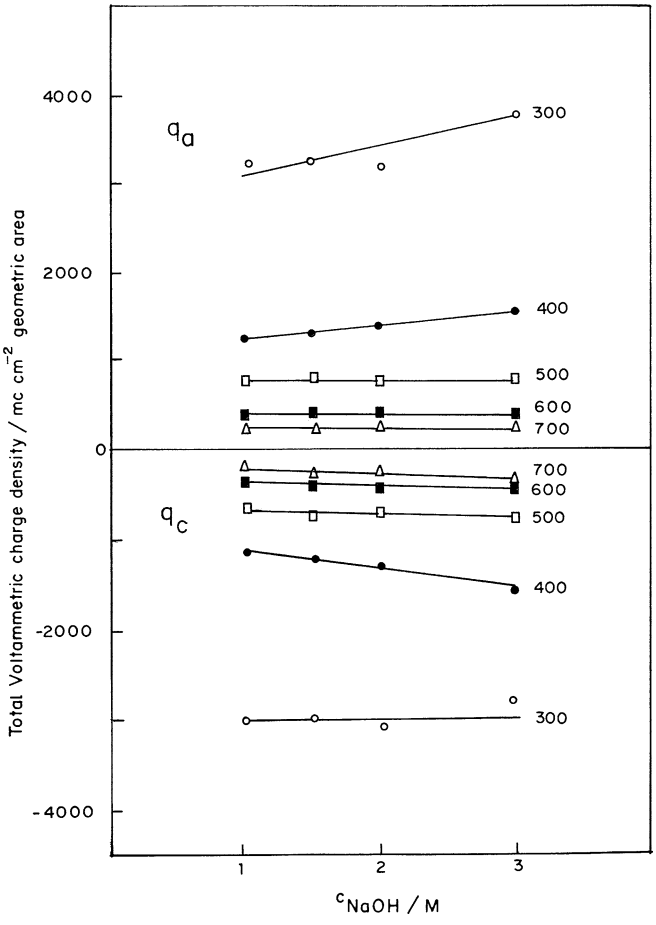

Fig. 3 Dependence of total voltammetric surface charge densities normalized over electrode geometric area, q_a and q_c, on NaOH concentration for RuO_2-PVC film electrodes of different oxide preparation temperatures (°C) indicated in the figure. q_a and q_c were obtained integrating the CV curve over the complete potential interval −1,100 to 450 mV (SCE) for 5 mV s^{-1} sweep rate

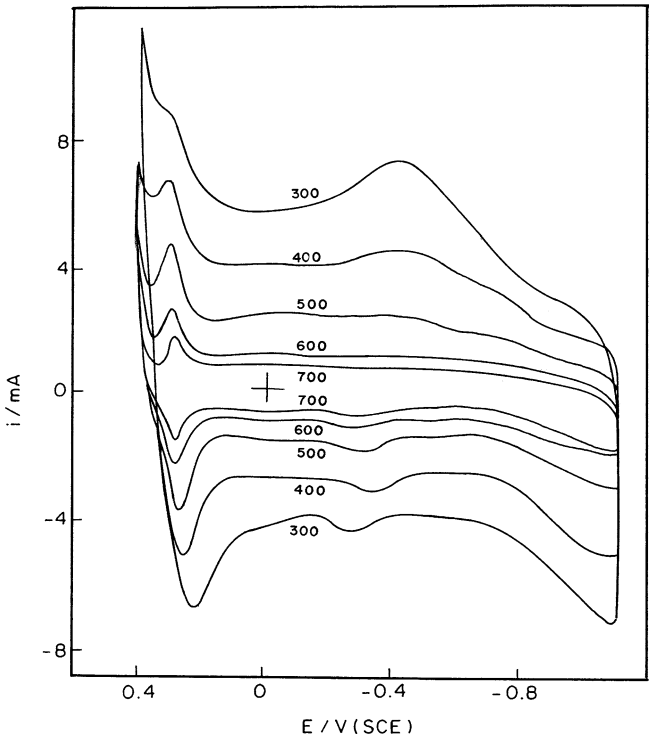

Fig. 4 Cyclic voltammograms in 3 M NaOH for RuO_2-PVC film electrodes of different oxide preparation temperatures (°C) indicated in the figure. Sweep rate 10 mV s^{-1}. Electrode geometric area = 0.0707 cm^2

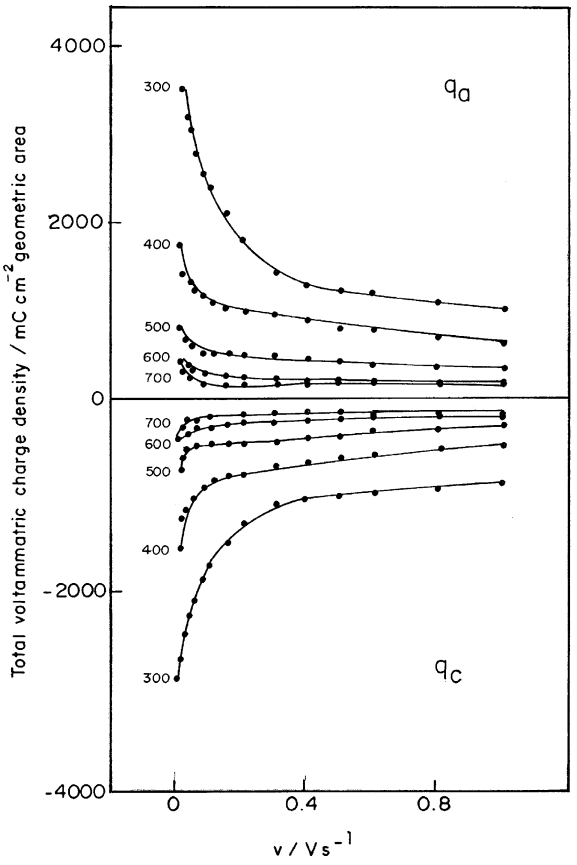

Fig. 5 Variation of total voltammetric surface charge densities normalized over electrode geometric area, q_a and q_c, with potential sweep rate in 3 M NaOH for RuO_2-PVC film electrodes of different oxide preparation temperatures (°C) indicated in the figure

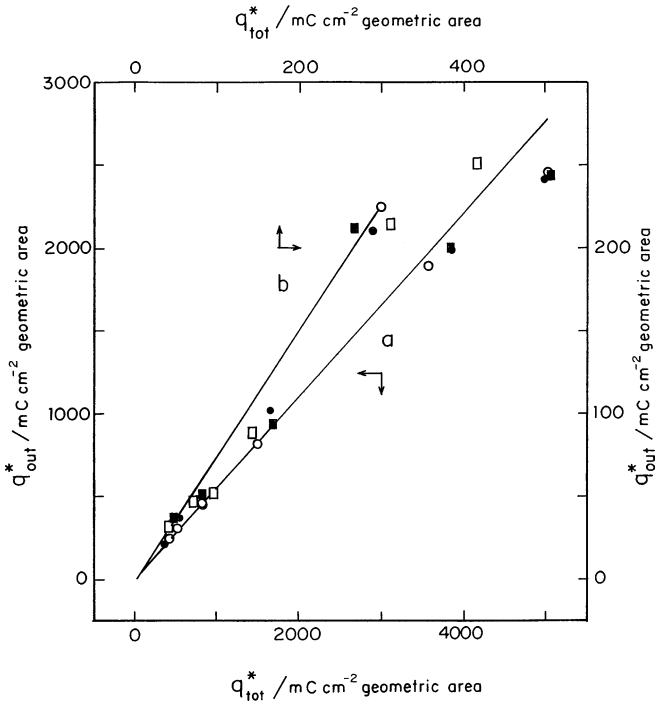

Fig. 6 q^*_{out} versus q^*_{tot} plots for RuO_2-PVC film electrodes of different oxide preparation temperatures in NaOH solutions of different concentrations (M): (open circle) 1; (*filled circle*) 1.5; (*open square*) 2; (*filled square*) 3. Curve (a): for 300 to 600°C electrodes and curve (b): for 700°C electrode

that is straight forwardly accessible to OH^- ion exchange.

$$q_a = q^*_{out} + \text{constant2}\left(\frac{1}{v^{1/2}}\right) \quad (7)$$

Once q^*_{tot} and q^*_{out} are calculated, as above, q^*_{in} is got remembering that

$$q^*_{tot} = q^*_{out} + q^*_{in} \quad (8)$$

Figure 6 illustrates a plot of q^*_{out} versus q^*_{tot} for all the five electrodes in the four NaOH solutions. It is interesting to note that the points gather around a single line of slope ~0.55 for all low temperature electrodes viz., 300 to 600°C (curve (a)), irrespective of NaOH concentration, indicating that the whole surface is almost equally divided between outer and inner regions. On the other hand, for 700°C electrode the ratio q^*_{out}/q^*_{tot} is closer to unity (0.78) as clearly shown in the expanded line (curve (b)), implying that this electrode possesses negligibly small inner area ($q^*_{in} \sim 25\%$), as already inferred from constant q-v data in Fig. 5. The physicochemical data for the RuO_2 samples collected from Ref. [33, 42] are summarized in Table 1. The pore-specific volume data from BET measurements are sufficient for the discussion at this stage. The pore-specific volume being larger for low temperature samples, 300 to 600°C, and smaller for the 700°C sample amply support the q^*_{out}/q^*_{tot} results that 300 to 600°C materials are more porous, but the 700°C sample is not. As one can see later, this factor has a decisive effect on the electrocatalytic behavior of 700°C electrode towards glucose oxidation in possessing extended linear calibration range, compared to other low temperature electrodes.

Note that Ardizzone et al. [41] calculated q^*_{out} and q^*_{tot} for 300 to 500°C thermally prepared Ti/RuO_2 electrodes in 1 M $HClO_4$ and 1 M KOH. The correlation between q^*_{out} and q^*_{tot} was found to be linear only in $HClO_4$ solution with a slope ~ 0.55; whereas in KOH solution it was nonlinear with q^*_{out} decreasing more in KOH than in $HClO_4$ as the active site quantity increases. Such a behavior was explained in terms of rate of surface diffusion of proton-donating species, being faster in acid and slower in alkali solution. Our results in Fig. 6 indicate that q^*_{out} versus q^*_{out} is linear in alkaline solutions, 1 to 3 M NaOH, for 300 to 600°C RuO_2-PVC film electrodes. In other words, the presence of PVC constitutes a favorable microenvironment for faster surface diffusion of proton-donating species even in alkaline medium, the more the higher the active site concentration. The exact nature of this enhancement is not known but interaction between PVC and OH^- may be suspected.

Table 1 Physicochemical parameters of RuO_2 samples prepared at different temperatures[a]

RuO_2 preparation temperature (°C)	BET pore-specific volume (10^3 cm^3 g^{-1})	XRD average particle size (A^0)	SEM morphology	DTGA no. of moles of H_2O	XPS		EASA[b] (10^{+3} cm^2)	Γ^{c}_{s3} (mol cm^{-2})
					BE of Cl $2p_{3/2}$ (eV)	% Ru(VI)/Ru(IV)		
300	21.29	134	Sponge-like porous material	0.314	197.8	0.21	1.92	1.32×10^{-6}
400	10.79	154		0.173	197.5	0.27	1.52	1.54×10^{-6}
500	8.54	159		0.099	[d]	0.27	1.04	1.20×10^{-6}
600	9.55	119		0.067	[d]	0.32	0.51	7.22×10^{-7}
700	6.15	173	Large crystallites	0.042	[d]	0.27	0.41	8.21×10^{-7}

[a] From Ref. [33, 34]
[b] Calculated from small amplitude CV method in 1 M NaOH
[c] Surface excess of A3 peak (Ru(VII)/Ru(VI)) redox transition in 1 M NaOH
[d] Not detected by XPS

Catalytic glucose oxidation

Oxidation of glucose at RuO_2 (700°C)-PVC film electrode

The curve (a) of Fig. 7 shows the CV for the oxidation of 15 mM glucose at a RuO_2 (700°C)-PVC film electrode in 1 M NaOH. In Fig. 7, also included is the response of RuO_2 (700°C)-PVC film electrode in pure base electrolyte devoid of glucose (curve (b)). In presence of glucose, the anodic currents corresponding to both Ru(IV) oxidation to Ru(VI) (A2 peak) and Ru(VI) oxidation to Ru(VI1) (A3 peak) increased, while the cathodic peak current of C3 decreased and the C2 peak totally disappeared. It was observed that the peak currents of A2 and A3 increased steadily with glucose concentration. These are indications that the glucose oxidation at RuO_2 (700°C) electrode in NaOH may occur by mediation by surface-confined ruthenium redox species. There are several possibilities for the appearance of two oxidation peaks for the glucose oxidation at RuO_2 (700°C) electrode in 1 M NaOH solution. In the first place, note that the peaks are centered in the potential region of Ru(IV) to Ru(VI) oxidation and Ru(VI) to Ru(VII) oxidation. Apparently, both ruthenate Ru(VI) (at peak A2) and perruthenate Ru(VII) (at peak A3) are electroactive towards glucose oxidation. However, there are conflicting reports regarding the catalytically active surface species of RuO_2 electrode [15, 19, 20, 25–27], implying that the nature of the catalytic species is dependent on the type of the substrate molecule. For example, the perruthenate (Ru(VII)) surface group is regarded as active towards the oxidation of difficultly oxidizable compounds like benzyl alcohol [19, 25] and formic acid [20]. Both Ru(VII) and Ru(VI) have been proposed to be active for benzaldehyde [19], formaldehyde [20], and glucose [15]. In the case of ethanol, however, while Shieh and Hwang [26] have suggested that only Ru(VII) is active; Ru(VI) species has been identified to be the only active species by de Andrade et al. [27].

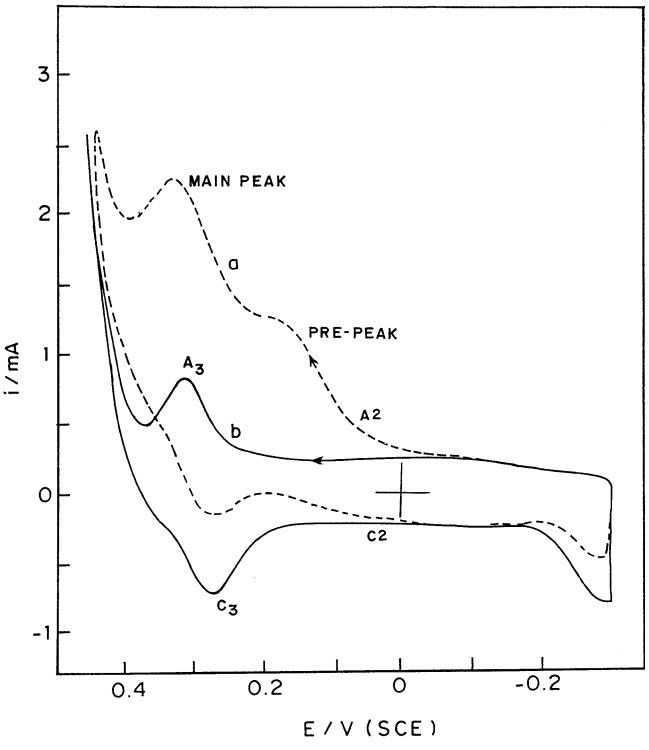

Fig. 7 Cyclic voltammograms of glucose at RuO_2(700°)-PVC film electrode in 1 M NaOH: (curve (a)) 15 mM glucose; (curve (b)) supporting electrolyte without glucose. Sweep rate 10 mVs^{-1}. Electrode geometric area = 0.0707 cm^2

It is well established that in solutions of pH < 13 the highest surface-oxidized form of ruthenium species that is generated during RuO_2 oxidation is only Ru(VI) within the potential range in which the supporting electrolyte is stable [19, 20, 25–27, 33]. Thus, the oxidation of glucose was carried out at RuO_2(700°C)-PVC electrode in pH 10.6 (borax + NaOH) buffer solution, to examine whether Ru(VI) species is catalytically active for glucose oxidation, and the results are presented in Fig. 8. RuO_2(700°C)-PVC electrode in pure base electrolyte shows two redox pairs of peaks (curve (a)):

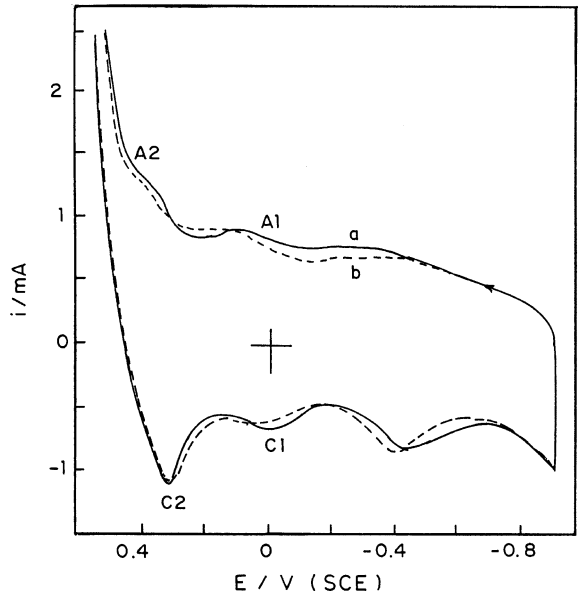

Fig. 8 Cyclic voltammograms of glucose at RuO_2(700°)-PVC film electrode in borax + NaOH solution of pH 10.6: (curve (a)) supporting electrolyte without glucose; (curve (b)) 15 mM glucose. Sweep rate 10 mV s^{-1}. Electrode geometric area = 0.1964 cm^2

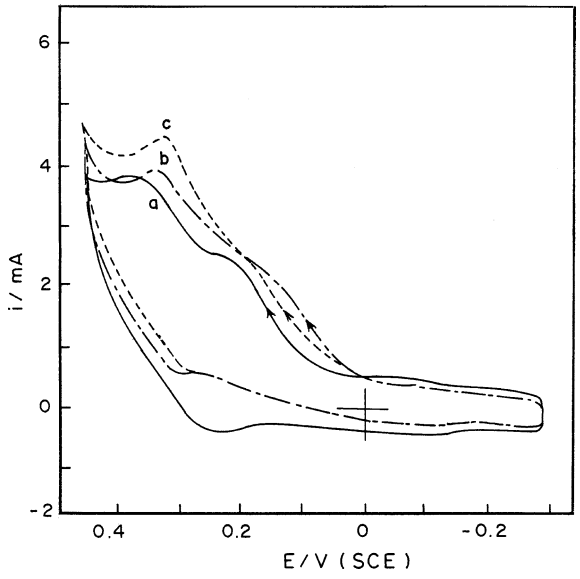

Fig. 9 Cyclic voltammograms of glucose and its derivatives at RuO_2(700°)-PVC film electrode in 1 M NaOH: (curve (a)) glucose; (curve (b)) fructose; (curve (c)) sodium gluconate. Substarte concentration 10 mM. Sweep rate 10 mV s^{-1}. Electrode geometric area = 0.1964 cm^2

A1/C1 corresponds to Ru(IV)/Ru(III) at $E_{1/2} \approx$ 0 mV and A2/C2 corresponds to Ru(VI)/Ru(IV) at $E_{1/2} \approx$ 340 mV. When glucose (10 mM) is added, the voltammogram is virtually unaffected (curve (b)), suggesting that Ru(VI) species is not catalytically active towards glucose oxidation. Therefore, the glucose oxidation peak observed for RuO_2(700°C)-PVC electrode in 1 M NaOH at lower potential 100–200 mV in Fig. 7 is not due to mediation by ruthenate Ru(VI), but it has a different origin. Note that the necessity of higher alkaline condition for the electrocatalytic oxidation of glucose was reported with RuO_2 carbon-paste electrode [14], and also with Ni [9, 10] and Co [11]. Thus, the glucose oxidation in alkaline solution occurs via redox mediation by Ru(VII) at higher potentials in the range 300 to 400 mV as follows:

$$\mathrm{Ru(VI)_{Sur}} \rightleftharpoons \mathrm{Ru(VII)_{Sur}} + e \tag{9}$$

$$2\mathrm{Ru(VII)_{Sur}} + \mathrm{G_{Sol}} \rightarrow 2\mathrm{Ru(VI)_{Sur}} + \mathrm{GL_{sol}} \tag{10}$$

where G denotes glucose and GL represents gluconolactone.

We may consider that the two oxidation peaks for glucose on RuO_2(700°C)-PVC electrode in 1 M NaOH, Fig. 7, correspond to successive oxidation of glucose substrate—the mechanism similar to that noticed with metal electrodes [1–3, 7]. On metal electrodes glucose is oxidized step-wise with the first peak at low potentials corresponding to the abstraction of α-hydrogen from glucose molecule followed by further oxidation at higher potential region. The abstraction of α-hydrogen in the case of glucose on metal electrodes was confirmed from oxidation studies with α-hydrogen lacking carbohydrates, like, sodium gluconate, fructose etc., which showed one-stage oxidation at higher potentials [2, 7]. But, on RuO_2 (700°C)-PVC electrode, we have observed experimentally, as shown in Fig. 9, that all these α-hydrogen-lacking carbohydrates are oxidized with two oxidation peaks similar to glucose oxidation. Besides, the intensity of both the anodic peaks does increase with increase in bulk concentration of these derivatives. This observation suggests that the first glucose oxidation peak on RuO_2 (700°C) electrode in 1 M NaOH (Fig. 7, curve (a)) is not connected with α-hydrogen abstraction, signifying that the glucose oxidation on RuO_2 does not proceed following the same mechanism as with metal electrodes.

We believe that the glucose oxidation peak at lower potentials on RuO_2, Fig. 7, may be an adsorption pre-peak as a result of the strong adsorption of the oxidized product, as well-documented in the polarography and CV literature [36]. The effect of potential sweep rate on the oxidation of glucose at the RuO_2 electrode confirms this proposal. With increase in scan rate, peak current increases for both the peaks (Fig. 10); however, the pre-peak increases at a faster rate than the main peak for several glucose concentrations (Fig. 10, inset (A)). Moreover, note that the peak current of the pre-peak increases linearly with v, i.e., $\partial i_{pa}/\partial(\log(v)) \approx 1$ (Fig. 10, inset (B)), typical of a surface electron transfer process. But, for the main peak, the peak current increases linearly with $v^{1/2}$, i.e., $\partial i_{pa}/\partial(\log(v)) \approx 0.5$, typical of diffusion-controlled electron transfer process.

Thus, in effect, the glucose oxidation at RuO_2 (700°C)-PVC film electrode in alkaline solution occurs via redox mediation by electrogenerated Ru(VII) in two

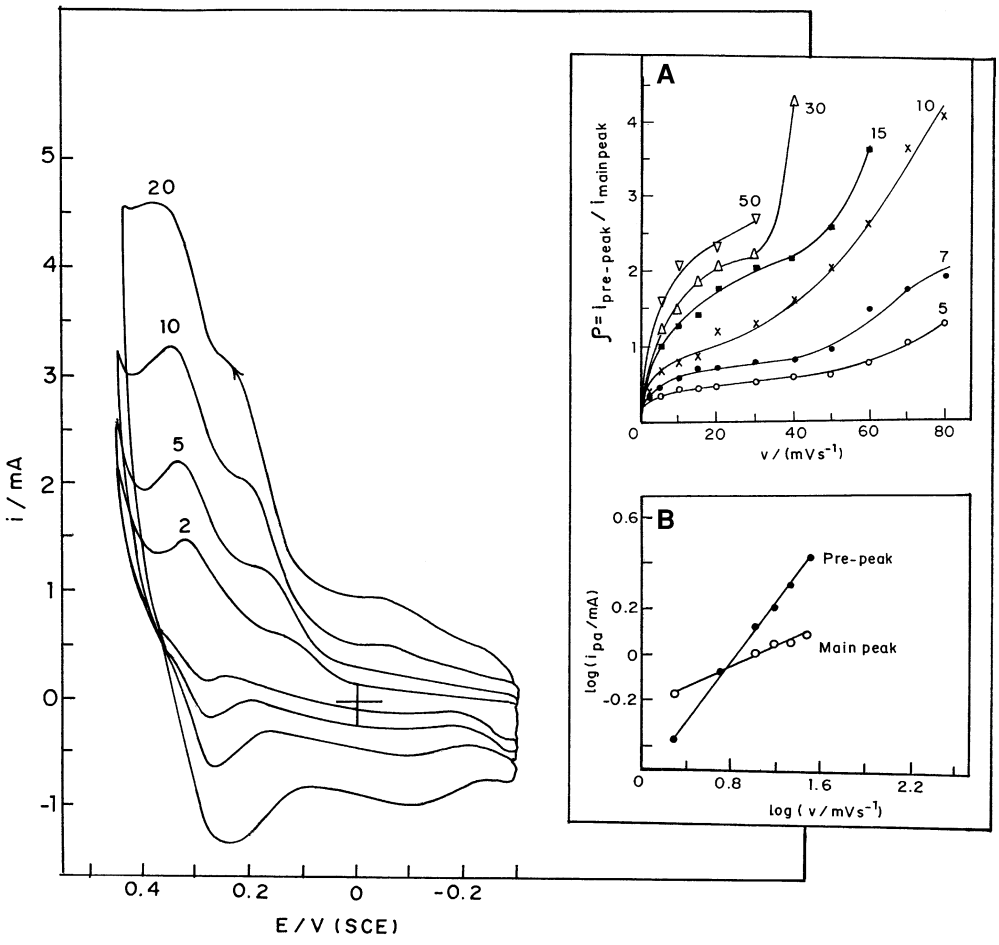

Fig. 10 Cyclic voltammograms of glucose at RuO_2(700°)-PVC film electrode in 1 M NaOH at various sweep rates (mV s^{-1}) indicated in the figure. Glucose concentration 15 mM. Electrode geometric area = 0.1964 cm^2 Inset (A): dependence of peak current ratio (ρ) of pre-peak to main peak on sweep rate for various glucose concentrations (mM) indicated in the figure Inset (B): Log(i_{pa}) versus log(v) plots for 15 mM glucose: (*filled circle*) pre-peak; (*open circle*) main peak

ways: one involving soluble forms of both the reactant and the product at the main peak in the potential region 300 to 400 mV (reaction (Eq, 10)), and the other involving strong product adsorption at the pre-peak in the potential region 100 to 200 mV (reaction (Eq. 11)).

$$2Ru(VII)_{Sur} + G_{Sol} \rightarrow 2Ru(VI)_{Sur} + GL_{Sol} \quad (10)$$

$$2Ru(VII)_{Sur} + G_{Sol} \rightarrow 2Ru(VI)_{Sur} + GL_{Ads} \quad (11)$$

Oxide preparation temperature effect on the catalytic oxidation of glucose

The oxide preparation temperature effect was investigated for 15 mM glucose oxidation in 1 M NaOH for all the five RuO_2-PVC film electrodes. Figure 11 shows comparative CVs recorded at $v = 10$ mV s^{-1} for the five electrodes. It is quite interesting to note that the pre-peak, which is present prominently with high temperature electrodes, decreases gradually with decrease in oxide preparation temperature and it is totally absent with 300°C electrode. The peak potential of the main catalytic peak is displaced towards more positive potentials as the preparation temperature decreases. This behavior suggests that the overall catalytic activity of the electrodes for glucose oxidation is higher for high temperature electrodes.

The efficiency of the oxide electrodes for glucose oxidation was characterized using the glucose oxidation current (i_{cat}) normalized over electrode geometric area (A_{geo}), i.e., the apparent electrochemical activity [25, 27, 28], $j_{cat} = i_{cat}/A_{geo}$. Figure 12A shows a plot of j_{cat} as a function of oxide preparation temperature. The j_{cat} data presented in Fig. 12(A) correspond to oxidation current measured at 350 mV from cyclic voltammogram recorded at $v = 1$ mV s^{-1} at a rotating electrode with 1,000 rpm for the oxidation of 15 mM glucose in 1 M NaOH at RuO_2-PVC film electrodes of different oxide preparation temperatures. It is clear that j_{cat} decreases with increase in oxide preparation temperature indicating that the low temperature RuO_2 electrodes (300–500°C) possess higher activity than the 600 and 700°C samples.

The j_{cat} parameter reflects changes in both morphologic (area) and intrinsic electrocatalytic effects. To compare the real catalytic activity of the different electrodes, one must separate the individual contributions. It is possible to eliminate morphological effects from the electrochemical response by dividing the oxidation current by the electrochemically active surface area

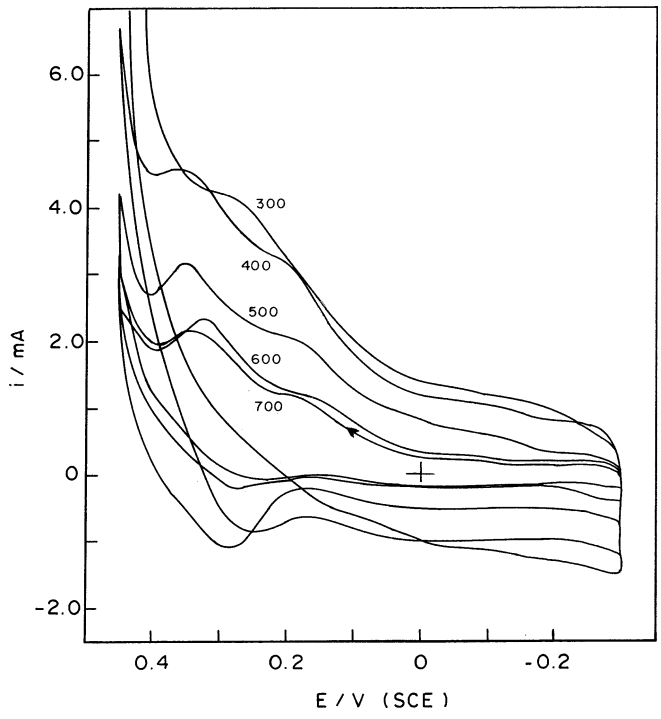

Fig. 11 Cyclic voltammograms of glucose in 1 M NaOH at RuO_2-PVC film electrodes of different oxide preparation temperatures (°C) indicated in the figure. Sweep rate 10 mV s^{-1}. Electrode geometric area = 0.0707 cm^2

(EASA). The normalized oxidation current, free of area effects, is given by $j_{cat}' = i_{cat}/EASA$, and j_{cat}' as a function of preparation temperature is illustrated in Fig. 12B. EASA for each of the five electrodes was estimated from double-layer-charging curves in 1N NaOH using the small amplitude CV technique, as described in detail elsewhere [33], and the EASA for all the electrodes are listed in Table 1.

Figure 12B shows a trend reverse to that observed in Fig. 12A clearly evidencing that high-temperature-prepared RuO_2-PVC film electrodes have better intrinsic catalytic properties than the low temperature samples.

Now referring to Table 1, it shows that the high temperature sample, 700°C RuO_2, possesses smaller amount of Cl^- (XPS), higher Ru(VI) content (XPS), and smaller water content (DTGA), compared to low temperature sample, 300°C RuO_2. Basing on these data, the behavior of higher temperature RuO_2 electrodes showing better intrinsic catalytic activity can be associated with the following possibilities.

1. The pK_A of glucose being 12.28, the reactant molecule in alkaline solution is anionic [43]. Thus, its oxidation at a 300°C electrode may proceed with a higher activation energy due to the presence of submonolayer quantities of anionic Cl^- in the network structure of water in the surface layer of this electrode. Consequently, with the complete absence of Cl^- (Table 1), the 700° RuO_2 electrode can allow glucose oxidation reaction to occur at enhanced rates resulting in high electrocatalytic activity.
2. RuO_2 particles in solution are known to present with extensive hydration of surface oxyhydroxide groups [34, 40]. The lesser quantities of water for 700°C sample (Table 1) reflect that its surface is hydrated to a lesser extent (less hydrophilic). Near the surface of such an arrangement, the glucose molecule with its six –OH groups may form strong water-like network structure as a result of extensive interaction between –OH groups and the Ru metal sites at the oxide surface. Thus a stronger adsorption interaction, a prerequisite for a more facile electron transfer, can be envisaged between glucose and 700°C RuO_2 surface (than 300°C electrode).
3. Other explanations for high reactivity of the 500–700°C electrodes consider higher quantity of the precatalyst species, Ru(VI), identified with these samples (Table 1). These Ru(VI) species can support preferential adsorption of glucose oxidation products producing additional path for glucose oxidation in the form of adsorption pre-peak along with the main

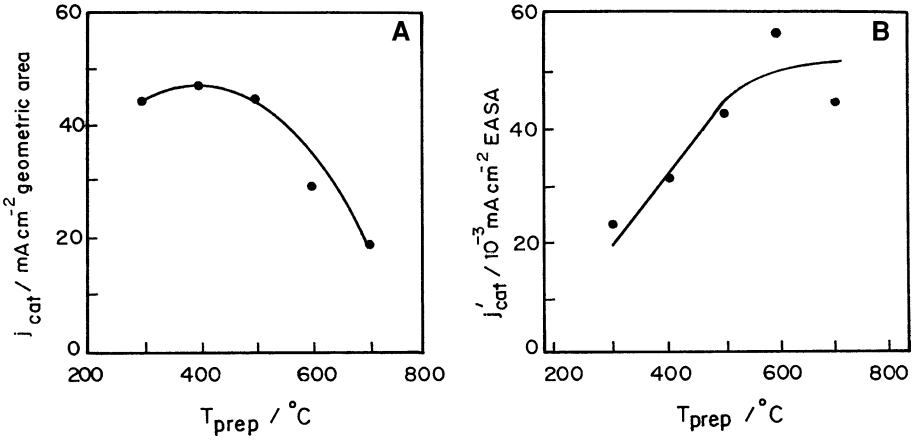

Fig. 12 **A** Catalytic current density normalized over electrode geometric area, j_{cat}, as a function of oxide preparation temperature in 1 M NaOH. **B** Catalytic current density normalized over electrochemically active surface area (EASA), j_{cat}', as a function of oxide preparation temperature in 1 M NaOH. For details see text

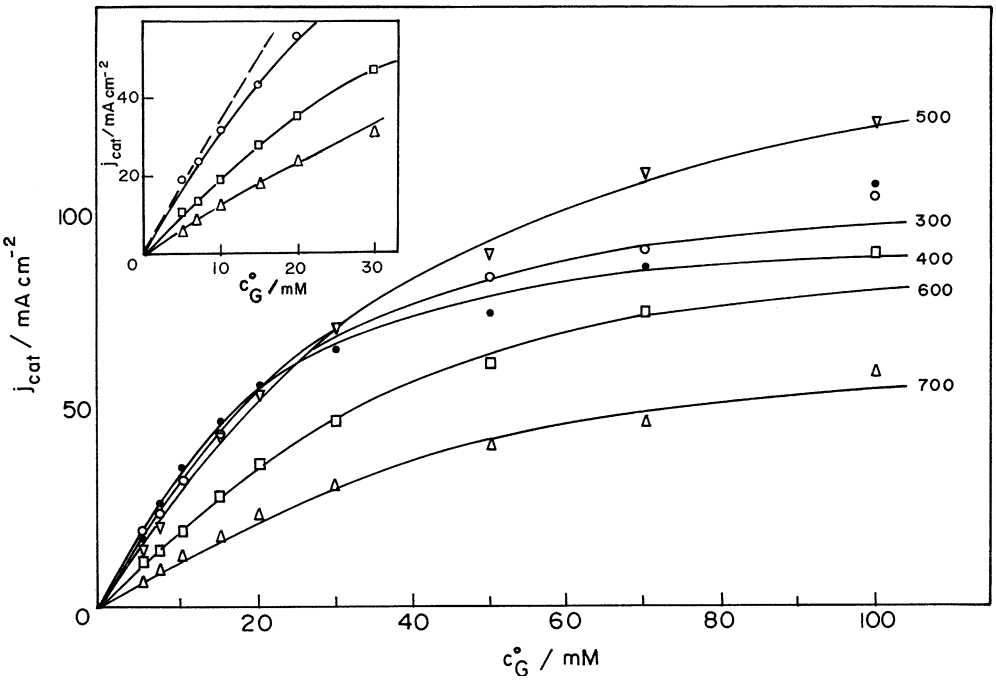

Fig. 13 j_{cat} variation with glucose concentration (c^0_G) in 1 M NaOH for RuO_2-PVC film electrodes of different oxide preparation temperatures (°C) indicated in the figure. Inset: variation of j_{cat} in the lower region of c^0_G

peak (Fig. 7), with overall higher activity of these electrodes.

Oxide preparation temperature effect on the linear calibration range

Figure 13 shows the plot between j_{cat} (measured at 350 mV) and glucose concentration (c^0_G) for various RuO_2 electrodes in 1 M NaOH. The data presented in Fig. 13 were obtained at a RDE rotated at 1,000 rpm and $v = 1$ mV s^{-1}. It may be noted that for all the electrodes the catalytic oxidation current increases with glucose concentration, but levels-off at higher concentration. It can, therefore, be inferred that glucose oxidation at all the RuO_2-PVC film electrodes follows saturation kinetics similar to that described by Michaelis–Menten (MM) reaction scheme involving the formation of a complex between the oxyruthenium surface species and dissolved glucose, which subsequently decomposes to generate the pre-catalyst and the product glucanolactone.

$$2\mathrm{Ru(VII)_{Sur}} + \mathrm{G_{Sol}} \overset{K_M}{\leftrightarrows} [2\mathrm{Ru(VII)}{-}{-}{-}\mathrm{G}]_{Sur} \overset{k_C}{\rightarrow} 2\mathrm{Ru(VI)_{Sur}} + \mathrm{GL_{Sol}} \quad (12)$$

One may write the corresponding equation as [15, 23]

$$\frac{1}{j_{cat}} = \frac{1}{nFk_c\Gamma_S} + \frac{K_M}{nFk_c\Gamma_S c^0_G} \quad (13)$$

where k_c (cm s^{-1}) and K_M (in mol dm^{-3}) are the MM kinetic constants, n the number of electrons transferred for oxidation of one molecule of glucose (here $n = 2$), Γ_s surface concentration of redox sites and F the Faraday constant. The behavior that glucose follows MM kinetics can be further confirmed by rea-

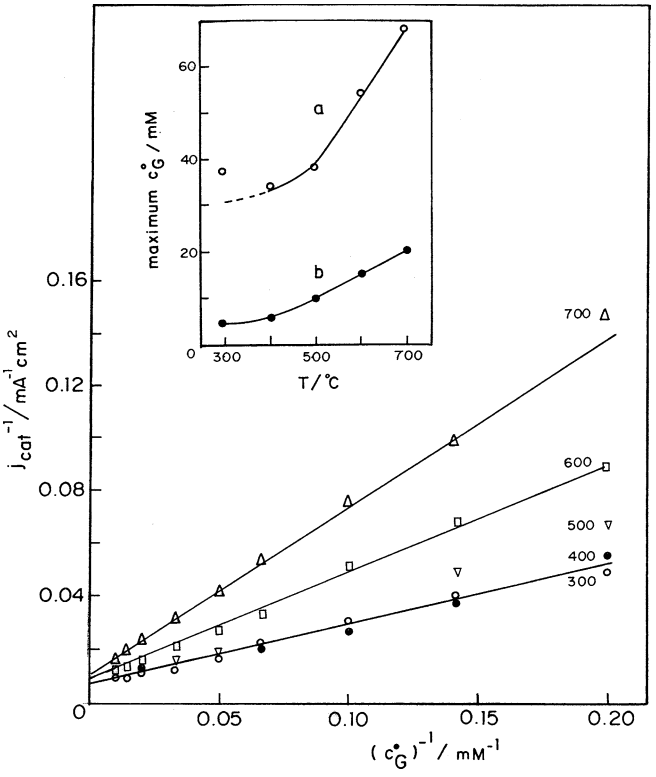

Fig. 14 Lineweaver-Burk plot (j^{-1}_{cat} versus $(c^0_G)^{-1}$) for the data in Fig. 13. Inset: Dependence of maximum c^0_G of linearity range on oxide preparation temperature (T/°C): (Curve a) predicted from Michaelis–Menten kinetic equation; (Curve b) experimental

sonably linear Lineweaver-Burke plots (j_{cat}^{-1} versus $(c_G^0)^{-1}$) for all the RuO_2 electrodes, as shown in Fig. 14, with

$$\text{Slope} = \frac{K_M}{nFk_c\Gamma_S} \tag{14}$$

$$\text{Intercept} = \frac{1}{nFk_c\Gamma_S} \tag{15}$$

The constants k_c and K_M were calculated from intercept and slope using $n = 2$ and Γ_s for each individual electrode, as listed in Table 1. Figure 14-inset shows that the calculated K_M, which signifies the maximum concentration up to which linearity between j_{cat} and c_G^0 is maintained, increases with oxide preparation temperature (curve (a)).

The above result is quite significant and important, since it predicts that the linear calibration range is more wider and extended to higher glucose concentrations for high temperature RuO_2 electrodes than for electrodes prepared at low temperatures. It is indeed true experimentally, as illustrated in Fig. 13-inset, which shows linear calibration plots between j_{cat} and c_G^0 over lower range of glucose concentrations. Note that the linear range for 700°C electrode is extended over 0 to 20 mM, 0 to 15 mM for 600°C electrode, but it is restricted to 0 to 5 mM for 300°C electrode. The experimentally observed maximum c_G^0 of linearity range as a function of oxide preparation temperature is included in Fig. 14-inset as curve (b).

The wider linearity region extended to higher glucose concentrations associated with 700°C RuO_2 electrode may be understood as due to its pores of smaller size (Table 1), which can cause restricted diffusion of the analyte towards active Ru(VII) sites resulting in active sites getting saturated only when glucose concentration level approaches higher values, a phenomena already noticed with enzyme electrodes using microporous and homogeneous membranes of different pore diameters employed as outer membranes [44]. Thus, as far as the application of RuO_2 as amperometric electrode for the estimation of glucose is concerned, the morphological effects rather than the intrinsic catalytic properties determine its performance.

Now referring to two sets of maximum c_G^0 values of linearity region, one experimentally observed and the other predicted from Eq. 13, Fig. 14-inset shows that experimental values (curve (b)) are always lower than the predicted values from MM Eq. 13 (curve (a)), for all the five electrodes. In other words, experiments indicate surface site saturation at relatively lower glucose concentration, whereas higher glucose concentrations are predicted to saturate as per MM Eq. 13. This is probably because MM Eq. 13 concerns only with uncomplicated idealized reaction (Eq. 12), which contains soluble forms of glucose and glucanolactone; but in reality, we know now that the glucose oxidation on RuO_2 electrodes is fairly complex occurring by two paths one involving soluble forms of glucose and glucanolactone (reaction (Eq. 12)) and the other involving strong product adsorption with the following MM reaction scheme (reaction (Eq. 16))

$$\begin{aligned} &2\text{Ru(VII)}_{\text{Sur}} \\ &+ \text{G}_{\text{Sol}} \overset{K_{M'}}{\leftrightarrows} [2\text{Ru(VII)}---\text{G}]_{\text{Sur}} \overset{k'_C}{\rightarrow} 2\text{Ru(VI)}_{\text{Sur}} \\ &+ \text{GL}_{\text{Ads}} \end{aligned} \tag{16}$$

with K_M' and k_c' as the corresponding MM kinetic constants. This product adsorption reaction can additionally contribute, and higher oxidation current can be registered in experiments leading to surface site saturation at relatively low glucose concentrations. This explanation is supported by the observation in Fig. 14-inset that the difference in c_G^0 between the two sets of values is larger for high temperature electrodes, because only at these electrodes the strong product adsorption (pre-peak) is more pronounced.

Conclusions

1. RuO_2-PVC film electrodes, fabricated using RuO_2 powders prepared at five different temperatures, viz., 300, 400, 500, 600 and 700°C, showed in high alkaline media 1 to 3 M NaOH three redox pairs Ru(IV)/Ru(III), Ru(VI)/Ru(IV) and Ru(VII)/Ru(VI) exhibiting non-Nerntian behavior with $[\partial E_{1/2}/\partial \log(c_{OH})]$ shift of −85, −82, and −95 mV, respectively, similar to traditionally prepared RuO_2/Ti electrodes.
2. Both the redox pairs Ru(VI)/Ru(IV) and Ru(VII)/Ru(VI) are associated with repulsive interaction among the redox sites in the surface layer with corresponding interaction terms $r_{A2} = -4.40\times 10^7$ cm^2 mol^{-1} and $r_{A3} = -2.16\times 10^6$ cm^2 mol^{-1}, respectively, in 3 M NaOH.
3. Estimation of q^*_{tot}, q^*_{out}, q^*_{in} for all the five electrodes shows that the low temperature electrodes viz., 300 to 600°C, are associated with almost equally distributed outer and inner active sites, whereas the 700°C electrode possesses fewer inner active surface sites, in total agreement with pore-specific volume data from BET measurements.
4. The glucose oxidation on RuO_2 does not follow the same mechanism as on metal electrodes. Here glucose undergoes oxidation via redox mediation by electrogenerated Ru(VII) in two ways: one involving soluble forms of both the reactant and the product, and the other involving strong product adsorption, with the latter process more pronounced and persistent for high temperature RuO_2-PVC film electrodes.
5. The effect of oxide pyrolysis temperature of $RuCl_3.nH_2O$ revealed that high-temperature-prepared RuO_2-PVC film electrodes have poorer apparent electrochemical activity, but better intrinsic electrocatalytic activity compared to the low temperature samples. It appears that smaller amount of

Cl^- and higher Ru(VI) content (from XPS measurements), and smaller water content (from DTGA measurements) associated with high temperature RuO_2 samples are responsible.

6. The high-temperature-prepared RuO_2 electrodes exhibit more wider linear calibration range extended to higher glucose concentrations, and this is intimately connected to their lesser porosity and pores of smaller size (from BET measurements), which favor restricted-diffusion of the analyte and delayed-saturation of their active sites only at higher glucose concentrations.

Acknowledgements The research was financially supported by the University Grants Commission, New Delhi in the form of research fellowship to VD, which the authors gratefully acknowledge.

References

1. Vassilyev YuB, Khazova OA, Nikolaeva NN (1985) J Electroanal Chem (a) 196:105; (b) 196:127
2. Popovic KDj, Tripkovic AV, Adzic RR (1992) J Electroanal Chem 339:227
3. Largeaud F, Kokoh KB, Beden B, Lamy C (1995) J Electroanal Chem 397:261 and the references cited therein
4. Luo MZ, Baldwin RP (1995) J Electroanal Chem 387:87
5. Torto N, Ruzgas T, Garton L (1999) J Electroanal Chem 464:252
6. Larew LA, Johnson DC (1989) J Electroanal Chem 262:167
7. Hsiao MV, Adzic RR, Yeager EB (1996) J Electrochem Soc 143:759
8. DeMott Jr JM, Tougas TP, Jahngen EGE (1998) Electroanalysis 10:836
9. Fleishman M, Korinek K, Pletcher D (1971) J Electroanal Chem 31:39
10. Stitz A, Bucbberger W (1994) Electroanalysis 6:251
11. Cataldi TRI, Guerriei A, Casella IG, Desimoni E (1995) Electroanalysis 7:305
12. Santos LM, Baldwin RP (1987) Anal Chem 59:1766
13. Zhang X, Chan KY, You J, Lin Z, Tseung ACC (1997) J Electroanal Chem 430:147
14. Wang J, Taha Z (1990) Anal Chem 62:1413
15. Lyons MEG, Fitzerald CA, Smyth MR (1994) Analyst 119:855
16. Dharuman V, Chandrasekara Pillai K (1997) Indian. J Chem Tech 4:25
17. Dharuman V, Chandrasekara Pillai K (1999) Bull Electrochem 15:476
18. Gorski W, Kennedy RT (1997) J Electroanal Chem 424:43
19. Burke LD, Healy JF (1981) J Electroanal Chem 124:327
20. O'Sullivan EJM, White JR (1989) J Electrochem Soc 136:2576
21. Leech D, Wang J, Smyth MR (1990) Analyst 115:1447
22. Leech D, Wang J, Smyth MR (1991) Electroanalysis 3:37
23. Lyons MEG, Lyons CH, Michas A, Bartlett PN (1992) Analyst 117:1271
24. Wang J, Lin Y (1994) Electroanalysis 6:125
25. Lin SM, Wen TC (1995) J Appl Electrochem 25:73
26. Shieh DT, Hwang BJ (1995) J Electrochem Soc 142:816
27. de Andrade AR, Donate PM, Alves PPD, Fidellis CHV, Boodts JFC (1998) J Electrochem Soc 145:3839
28. Zanta CLPS, de Andrade AR, Boodts JFC (1999) Electrochim Acta 44:3333
29. Wu J, Suls J, Sansen W (2000) Electrochem Commun 2:90
30. Panic VV, Dekanski AB, Vidakovic TR, Miskovic-Stankovic VB, Javanovic BZ, Nikolic BZ (2005) J Solid State Electrochem 9:43
31. Trasatti S, Lodi G (1981) Properties of conductive transition metal oxides with rutile type structure. In: Trasatti S (ed) Electrodes of conductive metallic oxides, Part A. Elsevier, Amsterdam, pp 301–358
32. Trasatti S (1994) Transition metal oxides: versatile materials for electrocatalysis. In Lipkowski J, Ross PN (eds) The electrochemistry of novel materials. VCH, New York, pp 207–295
33. Senthil Kumar A, Chandrasekara Pillai K (2000) J Solid State Electrochem 4:408 and references therein
34. Lyons MEG, Burke LD (1987) J Chem Soc Faraday Trans I 83:299
35. Scholz F, Meyer B (1998) Voltammetry of solid microparticles immobilised on electrode surfaces. In: Bard AJ, Rubinstein I (eds) Electroanalytical chemistry, vol 20. Dekker, New York, p 1–86
36. Bard AJ, Faulkner LR (1980) Electrochemical methods. Wiley, New York
37. Brown AP, Anson FC (1967) Anal Chem 49:1589
38. Smith DF, Willman K, Kuo K, Murray RW (1979) J Electroanal Chem 95:217
39. Ilangovan G, Chandrasekara Pillai K (1997) Langmuir 13:566
40. Furlong DN, Yates DE, Healy TW (1981) Fundamental properties of the oxide/aqueous solution interface. In: Trasatti S (ed) Electrodes of conductive metallic oxides, Part B. Elsevier, Amsterdam, pp 367–432
41. Ardizzone S, Fregonara G, Trasatti S (1990) Electrochim Acta 35:263
42. Senthil Kumar A (1998) Ph.D Dissertation, Department of Physical Chemistry, University of Madras, Chennai, India
43. Marioli JM, Kuwana T (1992) Electrochim. Acta 37:1187
44. Maines A, Asworth D, Vadgama P (1996) Anal Chim Acta 333:223